Chaos, Solitons and Fractals 135 (2020) 109726

Contents lists available at ScienceDirect

Chaos, Solitons and Fractals

Nonlinear Science, and Nonequilibrium and Complex Phenomena

journal homepage: www.elsevier.com/locate/chaos

Frontiers

EFFECT of colored noise on the generation of seismic fault MOVEMENT: Analogy with spring-block model DYNAMICS

Srđan Kostić [a,*], Nebojša Vasović [b], Kristina Todorović [c], Igor Franović [d]

[a] Geology Department, Water Institute "Jaroslav Černi", Jaroslava Černog 80, 11226 Belgrade, Serbia
[b] Department of Applied Mathematics, University of Belgrade Faculty of Mining and Geology, Serbia
[c] Department of Physics and Mathematics, University of Belgrade Faculty of Pharmacy, Serbia
[d] Scientific Computing Lab, University of Belgrade, Institute of Physics, Serbia

ARTICLE INFO

Article history:
Received 27 January 2020
Accepted 2 March 2020
Available online 3 May 2020

Keywords:
Correlated noise
Correspondence with real measurements
Bifurcation
Regimes of fault motion dynamics

ABSTRACT

In present paper authors examined the effect of colored noise on the onset of seismic fault motion. For this purpose, they analyze the dynamics of spring-block model, with 10 all-to all coupled blocks. This spring-block model is considered as a collection of fault patches (with the increased rock friction), which are separated by the material bridges (more petrified parts of the fault). In the first phase of research, authors confirm the presence of autocorrelation in the background of seismic noise, using the measurement of real fault movement, and the recorded ground shaking before and after an earthquake. In the second stage of the research, authors firstly develop a mean-field model, which accurately enough describes the dynamics of a starting block model, with the introduced delayed interaction among the blocks, while colored noise is assumed to be generated by Ornstein-Uhlenbeck process. The results of the analysis indicate the existence of three different dynamical regimes, which correspond to three regimes of fault motion: steady stationary state, aseismic creep and seismic fault motion. The effect of colored noise lies in the possibility of generating the seismic fault motion even for small values of correlation time. Moreover, it is shown that the tight connection between the blocks, i.e. fault patches prevent the occurrence of seismic fault motion.

1. Introduction

Significance of seismic noise study in seismological research lies in the possibility of reliable subsurface tomography using the records on ambient seismic noise [1]. In particular, numerous field studies confirmed that ratio of horizontal to vertical component of ambient noise gives solid data on the subsurface geology in areas with low seismicity or even in aseismic areas [2]. However, none of the previous studies dealt with the effect of noise on the fault movement. Reason for this lies in inaccessibility of the fault zone to direct measurements, both of ambient noise and the fault movement. These measurements are only possible in deep boreholes, near the active fault zones, like in the case of fault movement directly measured at the Driny cave, MaleḰarpaty mts in Slovakia [3], or in the 3 km deep borehole that cuts through the San Andreas fault system within the SAFOD research project [4]. Also, the effect of noise on generation of seismic fault movement is impossible to prove by the in situ measurements. For these reasons, fault motion is usually examined by modeling in laboratory conditions, whereby simulations are commonly conducted in two ways: either by observing the behavior of an array of blocks (starting from the Burridge-Knopoff model), or by analysis of the motion between the two plates, whose contact is simulated by an assemblage of real or artificial grains. In these conditions, it is possible to simulate movement along the fault, including all the accompanying effects. Nevertheless, as far as authors are aware, effect of noise on fault motion has not been examined in laboratory conditions so far.

However, mathematical expressions which are used to describe the dynamics of such systems allow one to examine different effects, at least from a theoretical viewpoint. Regarding the effect of noise, in our previous work [5] we examined the dynamics of an array of 100 blocks under the effect of random seismic noise. In that case, assumption of random nature of seismic noise came from the two sources. Firstly, we examined the real observed GPS measurements of fault movement at the ground surface at several stations within the San Andreas fault zone, for which we established to have the properties of stochastic time series. Secondly,

* Corresponding author.
E-mail address: srdjan.kostic@jcerni.rs (S. Kostić).

https://doi.org/10.1016/j.chaos.2020.109726

we wanted to examine the effect of permanent background seismic noise, so it was natural to assume its random nature. However, what if the noise along the fault zone or in its immediate vicinity is correlated? Justification for this lies in existence of many potential sources of colored (correlated) noise: reservoir charging/discharging, penetration of sound waves emitted by neighboring fault motion, close earthquakes or explosion, ocean waves and tides, etc. Another source of colored noise could come from the pre-processing of the acquired measurements. In particular, recorded time series could be represented as a combination of a deterministic signal, i.e. convenient combination of sine and cosine wave, with the remaining stochastic residuals, which always have certain level of autocorrelation. All these factors could generate correlated oscillations of small amplitude with respect to the scale of fault motion.

In our previous work on the effect of random noise on the fault motion, we showed that when fault is in inter-seismic stage, near the boundary to the co-seismic regime, even random noise with very small amplitude could generate the transition to co-seismic fault motion. Regarding the possible multiple sources of colored seismic noise, in present paper we want to examine whether correlated noise could be also responsible for earthquake nucleation. For this purpose, we invoke the method of mean-field approximation, which enables us the reduction of large stochastic system to the simple deterministic system which could be further analyzed by applying standard local bifurcation analysis.

Presented research is performed with two main goals. Firstly, we want to show that in situ recorded fault motion is stochastic per se, and that the stochastic part of displacement time series could be treated as colored noise. Secondly, we wish to estimate the impact of colored noise on the generation of instability, i.e. on the occurrence of seismic fault motion. For the former, we invoke the joint deterministic-stochastic approach based on traditional Box-Jenkins method, while for the latter we perform the local bifurcation analysis of the mean-field approximated starting system of 10 blocks in a spring-block array along a single direction.

2. Colored noise in situ

In order to justify the introduction of the colored seismic noise in fault motion model, one needs to confirm the existence of colored noise in rela conidtions within the Earth's crust. In present case, we analyze the following datasets based on the real measurements:

(1) Strike-slip fault movement directly measured at the two points in Driny cave, Male ́Karpaty mts in Slovakia [3] (Fig. 1a),
(2) Ambiental noise measurements before and after the earthquake on 8th September 2015 at the BKS station (Byerly Seismogrpahic Vault, Berkley) (Fig. 1b).

In case (1) we show that once the estimation model of the fault movement is established, estimation error is autocorrelated, indicating the possibility of the existence of the colored noise. In case (2) we show that ambiental noise before and after the quake is autocorrelated.

Analysis of the measurement results shown in Fig. 1a indicates that the real observed time series could be well described by the following models in a general form of Fourier series sums of sine and cosine functions:

$$y = a_0 + a_1 \cdot \cos(\omega \cdot t) + b_1 \cdot \sin(\omega \cdot t) + a_2 \cdot \cos(2 \cdot \omega \cdot t) + b_2 \cdot \sin(2 \cdot \omega \cdot t) + \ldots \tag{1}$$

where a_i and b_i denote Fourier coefficients, and ω is the average oscillation freuqency. Coefficients and frequencies of the resulting models for estimation of displacements at the locations Driny 1 and Driny 3 are given in Table 1.

Using these equations, one could describe the observed horizontal strike-slip motion accurately enough (Fig. 2).

For the present case, properties of the estimation error are of special importance, since the presence of autocorrelation in residuals could indicate the existence of the colored noise in the background of the seismic movement. Indeed, the results of Durbin–Watson statistics indicate the presence of autoccorelation in the recorded noise ($<D_L$), according to reccommendations of Savin and White [7] (Table 2).

As for the recorded noise before and after the earthquake on 8th September 2015 at the BKS station (Byerly Seismogrpahic Vault, Berkley), one can simply calculate the autocorrelation function, which, in present case, for both time series (before and after the earthquake) indicates the presence of autocorrelation (Fig. 3). It is clear that there is a significant autocorrelation for the first 8 and 7 lags, for time series before and after the earthquake, respectively, while t-statistics is higher than 2 for the first two lags in both cases.

Concerning the results of the aforementioned analysis, one could reasonably assume that noise in the background of fault movement could be considered as a colored noise.

3. Bifurcation analysis

A new model for seismic fault motion is suggested in a form of a single array spring-block model, described by a deterministic mathematical model with the included effect of colored noise. Analysis of such model is conducted using the standard local bifurcation analysis, which is applied for the analysis ofthe deterministic mean-field system instead of the starting stochastic model. It is shown that both models display qualitative similar dynamics.

Earthquake fault motion is examined by analysis of dimensionless all-to-all coupled spring-slider model with 10 units, whose dynamics is described by the following set of stochastic delay differential equations (SDDEs):

$$\begin{aligned}
\dot{x}_i(t) &= y_i(t) \\
\dot{y}(t) &= -x_i(t) + \Phi(y_i + \nu) - \Phi(\nu) \\
&\quad + \frac{K}{N}\left(x_j(t-\tau) - x_i(t)\right) + Z_i(t) \\
dZi(t) &= -\frac{Z_i}{\varepsilon}dt + \sqrt{\frac{2D}{\varepsilon}}dW_i
\end{aligned} \tag{2}$$

where x_i and y_i represent displacement and velocity of the i th block, respectively, K is constant of spring connecting the blocks, Φ stands for the friction force, τ is time delay and ν is nondimensional pulling background velocity. $Z_i(t)$ is an Ornstein-Uhlenbeck process, and terms $\sqrt{(2D/\varepsilon)}dWi$ represent stochastic increments of independent Wiener process, i.e. dW_i satisfy: $E(dWi)=0$, $E(dW_idW_j)=\delta_{ij}dt$, where $E()$ denotes the expectation over many realizations of the stochastic process. The noise correlation time ε and the intensity of noise D are parameters that can be varied independently. Colored noise generated by Ornstein-Uhlenbeck process with this parametrization is referred to as power-limited colored noise, since the total power of the noise (the integral over the spectral density of the process) is conserved upon varying the noise correlation time.

Friction force Φ is assumed to be only rate-dependent: $\Phi(V) = -(\mu_0 + a\ln(V))$ where V is the general notion for the friction arguments in (2).

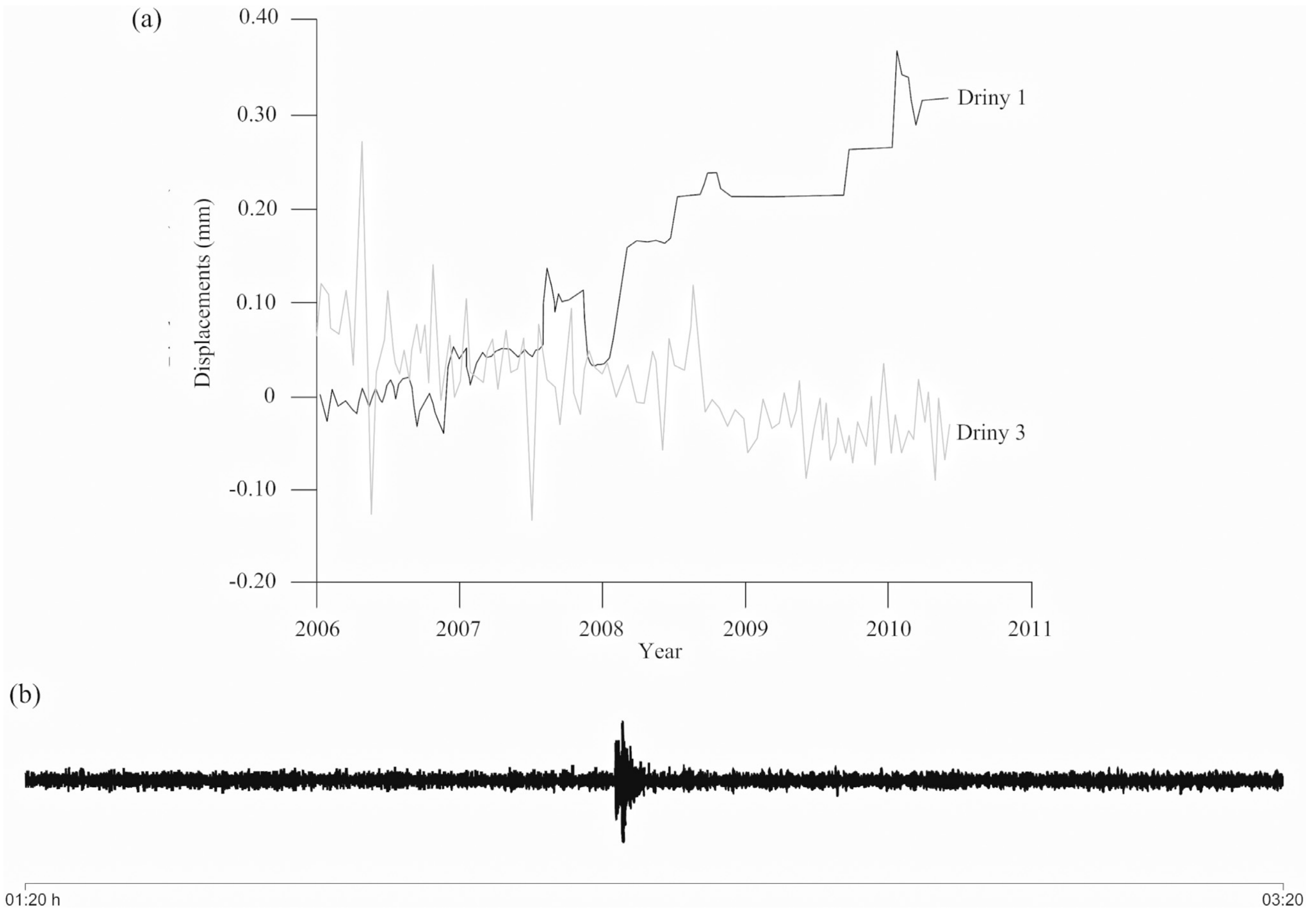

Fig. 1. (a) Horizontal strike-slip displacements along the faults at Driny Cave [3], (b) Permanent noise measurements before and after the earthquake at the Byerly Seismogrpahic Vault, Berkley [6].

Table 1
Fourier coefficients for deterministic models of fault movement of general form (1) based on the real observations atlocations Driny 1 and Driny 3.

Driny 1 (ω = 0.108)		Driny 3 (ω = 0.0205)									
a_0	0.139	a_0	0.012	a_9	−0.002	a_{17}	0.002	a_{25}	−0.004
a_1	0.116	a_1	0.002	b_9	−0.005	b_{17}	−0.002	b_{25}	0.0005
b_1	−0.063	b_1	0.038	a_{10}	0.002	a_{18}	−0.005	a_{26}	0.0003
a_2	0.031	a_2	0.007	b_{10}	0.006	b_{18}	−0.013	b_{26}	−0.0003
b_2	0.033	b_2	0.0280	a_{11}	0.002	a_{19}	0.007	a_{27}	0.0002
a_3	−0.007	a_3	−0.001	b_1	−0.009	b_{19}	−0.013	b_{27}	−0.006
b_3	0.048	b_3	−0.0005	a_{12}	0.005	a_{20}	−0.001	a_{28}	−0.009
a_4	−0.005	a_4	0.003	b_{12}	0.011	b_{20}	−0.001	b_{28}	0.008
b_4	0.016	b_4	0.016	a_{13}	0.003	a_{21}	0.009	a_{29}	0.003
a_5	−0.015	a_5	−0.007	b_{13}	0.009	b_{21}	−0.0007	b_{29}	−0.0005
b_5	−0.009	b_5	0.017	a_{14}	0.005	a_{22}	0.002	a_{30}	0.002
a_6	0.001	a_6	−0.006	b_{14}	0.009	b_{22}	0.013	b_{30}	−0.0006
b_6	−0.004	b_6	0.004	a_{15}	−0.011	a_{23}	−0.004	a_{31}	0.0089
a_7	0.008	a_7	−0.009	b_{15}	0.017	b_{23}	0.006	b_{31}	0.002
b_7	−0.006	b_7	0.019	a_{16}	−0.014	a_{24}	−0.004	a_{32}	0.002
a_8	−0.011	a_8	−0.006	b_{16}	−0.011	b_{24}	0.005	b_{32}	0.004
b_8	0.008	b_8	−0.011						

Table 2
Results of Durbin–Watson test for testing the presence of autocorrelation in residuals of the models in general form (1) and with the coeeficients given in Table 1.

Recording location	Durbin–Watson statistic	D_L	D_U
Driny 1	0.485	1.696	1.727
Driny 3	0.527	1.807	1.820

In present paper, authors consider this spring-block model as a collection of fault patches mutually separated by the petrified zones (material bridges). This is the modified original model from [8]

Starting from the model (2), one could obtain the following mean-field model, which has qualitatively the same dynamics as

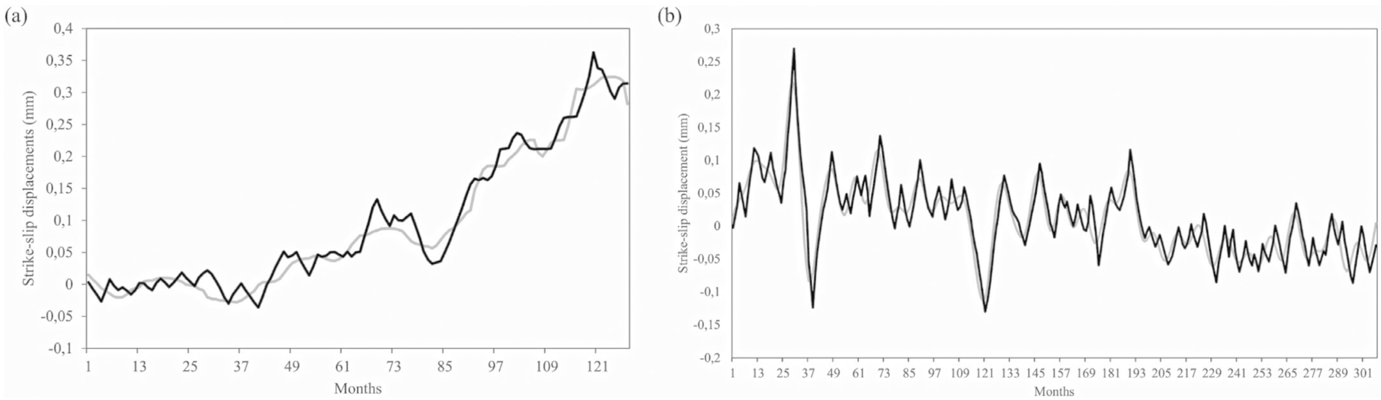

Fig. 2. Comparison of estimated motion and real observed fault movement. Black line stands for the recorded time series, while gray line indicates the result of estimation determinstic model.

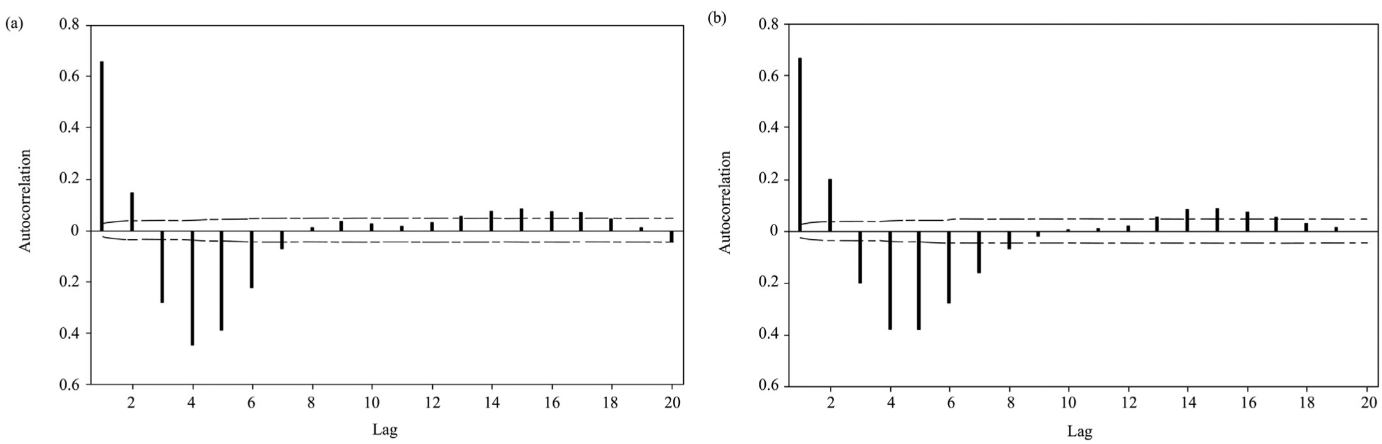

Fig. 3. Autocorrelation function for the time series before (a) and after (b) the earthquake on 8th September 2015 at the BKS station (Byerly Seismogrpahic Vault, Berkley), with the clear indication of the presence ofg autocorrelation.

the starting model (2):

$$
\begin{aligned}
&\dot{m}_x = m_y \\
&\dot{m}_y = -m_x - a\ln(m_y+\nu) + a\ln(\nu) + \tfrac{1}{2}\tfrac{a}{(m_y+\nu)^2}s_y \\
&\qquad + \tfrac{3}{4}\tfrac{a}{(m_y+\nu)^4}s_y{}^2 + K(m_x(t-\tau) - m_x) + m_z \\
&\dot{m}_z = -\tfrac{1}{\varepsilon}m_z \\
&\tfrac{1}{2}\dot{s}_x = U_{xy} \\
&\tfrac{1}{2}\dot{s}_y = s_y\left[-\tfrac{a}{m_y+\nu} - \tfrac{a}{(m_y+\nu)^3}s_y\right] - (K+1)U_{xy} + U_{yz} \\
&\dot{U}_{xy} = U_{xy}\left[-\tfrac{a}{m_y+\nu} - \tfrac{a}{(m_y+\nu)^3}s_y\right] - (K+1)s_x + s_y + U_{xz} \\
&\dot{U}_{xz} = U_{yz} - \tfrac{1}{\varepsilon}U_{xz} \\
&\dot{U}_{yz} = -U_{xz} - \tfrac{a}{m_y+\nu}U_{yz} - \tfrac{a}{(m_y+\nu)^3}s_yU_{yz} - KU_{xz} + D - \tfrac{1}{\varepsilon}U_{yz}
\end{aligned}
\tag{3}
$$

Detailed derivation of model (3) is given in Appendix.

Results of the numerical analysis of mean-field model (3) indicate the existence of three different dynamical regimes (Fig. 4–6):

- Equilibrium state, which manifests as steady stationary movement (corresponding to the steady regime of fault motion);
- Small-amplitude regular periodic oscillations (corresponding to the creep regime of fault motion);
- High-amplitude irregular oscillations (corresponding to the seismogenic fault motion).

From Fig. 4 one could identify the effect of correlation time ε on the dynamics of mean-filed model (2). In particular, with the increase of correlation time, second bifurcation curve vanishes, i.e. there are no high-amplitude oscillations. From the seismological point of view, this could indicate that degree of autocorrelation of background seismic noise could directly determine the type of transition from equilibrium state, i.e. creep regime of fault dynamics to low-amplitude oscillations (which could still not induce the seismogenic motion) or to high-amplitude irregular oscillations, whose amplitude progressively increases, which could be considered as the onset of the fault motion which produces the seismic waves responsible for surface soil shaking.

Regarding the effect of coupling strength K, it is clear from Fig. 5 that the increase of coupling strength further increases the impact of both time delay τ and friction a, and excludes the possibility of the occurrence of seismogenic fault motion. In particular, for higher values of K transition from equilibrium state to small amplitude oscillations, i.e. creep regime is possible even for higher values of friction a. From the seismological viewpoint, this means that the stronger interrelations between different patches of fault also induce the stronger role of friction. In the same time, it appears that for higher values of coupling strength, there is no possibility that seismogenic motion occur, since the second bifurcation curve (denoting the transition from creep regime to irregular seismogenic motion) vanishes.

However, this statement is valid only for the lower values of time delay. Indeed, one could see from Fig. 6 that high-amplitude irregular oscillations occur for higher values of time delay, i.e. $\tau > 5$. From the practical viewpoint, this means that the higher delay in interaction between the neighboring patches of fault – the more likely is to expect the onset of seismogenic fault motion. In other words, it seems that without the delay in nteraction, or with

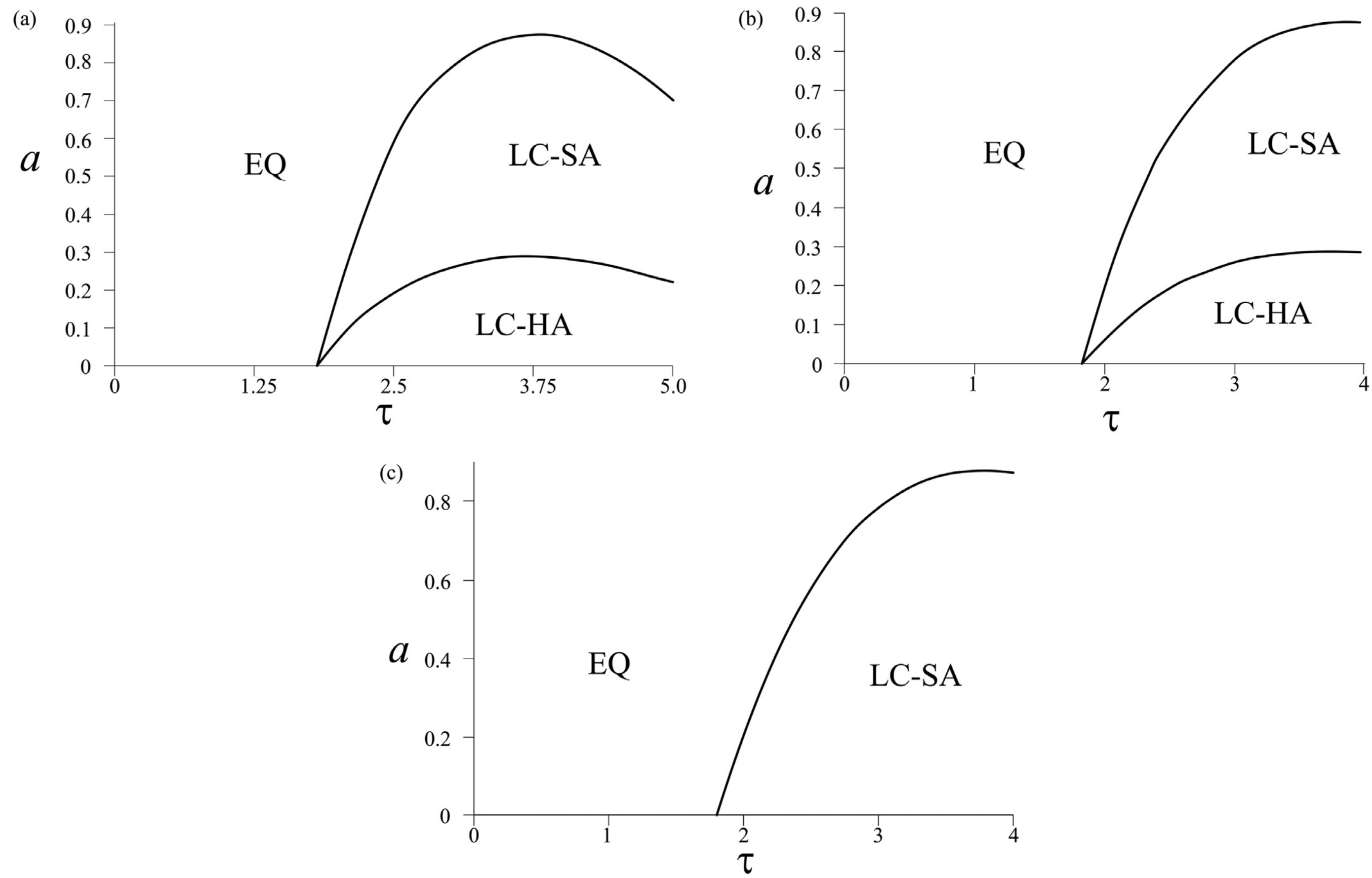

Fig. 4. Andronov-Hopf bifurcation diagram, displaying interaction of friction a and time delay τ, for different values of correlation time ε. While friction and delay are being varied, other parameters are being held constant for the mean-field model (3) in equilibrium state: $\mu_0 = 0.1$, $K = 1$, $D = 0.001$, $\nu = 1.2$. (a) $\varepsilon = 0.005$, (b) $\varepsilon = 0.5$, (c) $\varepsilon = 5.0$. EQ denotes the equilibrium state (steady stationary displacement), LC-SA stands for the periodic oscillations of small amplitude, while LC-HA denotes the high-amplitude irregular oscillations.

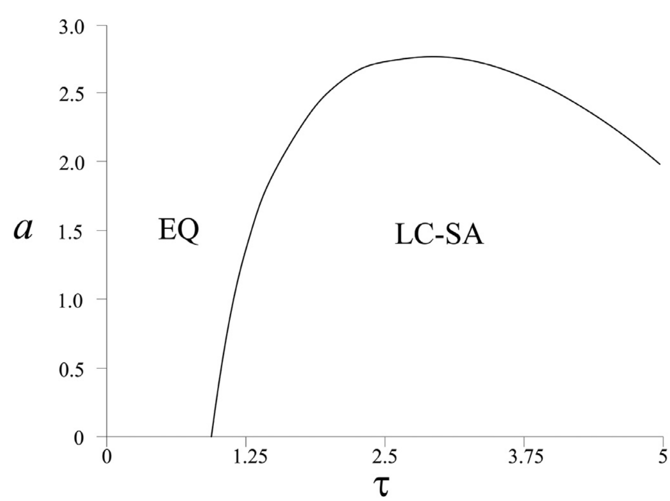

Fig. 5. Effect of coupling strength K on the dynamics of the mean-field model (3). While friction and delay are being varied, other parameters are being held constant for the mean-field model (2) in equilibrium state: $\mu_0 = 0.1$, $D = 0.001$, $\nu = 1.2$, $\varepsilon = 0.5$, $K = 5$. EQ denotes the equilibrium state (steady stationary displacement), while LC-SA stands for the periodic oscillations of small amplitude.

the small values of delay, the whole faults acts as a unique block, i.e. the fault patches are locked, preventing the irregular seismogenic motion to occur.

4. Discussion and conclusion

In present paper, authors examine the impact of the background colored seismic noise on the dynamics o fan active fault. Firstly, authors prove, by analyzing the measurement of the real fault displacement, that background seismic noise could be treated as the colored noise. This is done for the real two examples: (1) strike-slip fault movement directly measured at the two points in Driny cave, MaleḰarpaty mts in Slovakia [3]; (2) ambiental noise measurements before and after the earthquake on 8th September 2015 at the BKS station (Byerly Seismogrpahic Vault, Berkley). In the second phase of the research, authors investigated the fault dynamics by analyzing the mean-field model of all-to-all coupled blocks, with delayed interaction and with the assumed additive colored noise. The results obtained indicate the existence of three different dynamical regimes, all of which could have its correspondence with the real observed regimes of fault motion: (1) steady stationary state; (2) creep regime and (3) active seismogenic motion. Furthermore, the results indicate interesting effect of correlation time ε and coupling strength K on the onset of seismic fault motion. Higher values of ccorrelation time exclude the possibility of seismic fault motion, indciating the affect of strong impact of background seismic noise. Similarly, higher values of coupling strength also make seismic fault motion impossible to occur. In this case, when coupling strength is high, fault patches are interlocked and there is no possibility that irregular motion occur.

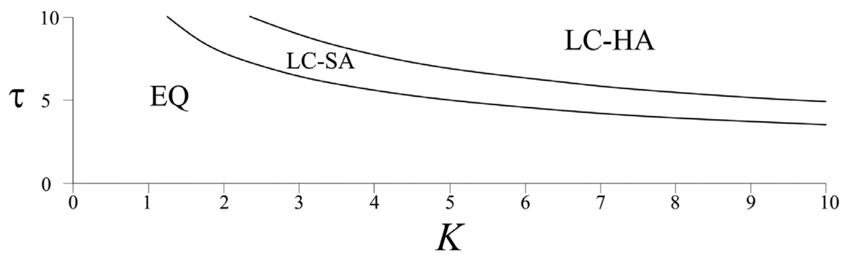

Fig. 6. Andronov-Hopf bifurcation diagram, displaying interaction of coupling strength K and time delay τ. While coupling strength and delay are being varied, other parameters are being held constant for the mean-field model (3) in equilibrium state: $\mu_0 = 0.1$, $D = 0.001$, $\nu = 1.2$, $a = 0.8$, $\varepsilon = 0{,}5$. EQ denotes the equilibrium state (steady stationary displacement), LC-SA stands for the periodic oscillations of small amplitude, while LC-HA denotes the high-amplitude irregular oscillations.

If one compares the effect of colored seismic noise, analyzed in this paper, and white seismic noise, analyzed in our previous paper [5], the difference lies in the following. For white background seismic noise, seismic fault motions could be expected to occur only in a bi-stable dynamical regime in the vicinity of a bifurcation curve provided that initial conditions along the fault are far from the equilibrium state (the case of active fault). On the other hand, introduction of colored noise brings more rich dynamical behavior, where colored noise with rather small correlation time (Fig. 4a) indicates the onset of seismic fault motion, with the increase of time delay.

Further research on this topic could evaluate the effect of colored noise in case when the interaction of neighboring blocks weakens with the mutual distance of the blocks, which is certainly closer to the real observed scenario.

Declaration of Competing Interest

The authors declare that they have no known competing financial interests or personal relationships that could have appeared to influence the work reported in this paper.

Acknowledgments

This research was partly supported by the Ministry of Education, Science and Technological Development of the Republic of Serbia (Contract nos. 176016 and 171017).

Appendix

By deriving the Taylor expansion of $\Phi(y_i(t)+\nu)$ in the vicinity of the mean values $(x_i, y_i, z_i) = (m_x, m_y, m_z) = (\lim\limits_{N\to\infty} \frac{1}{N}\sum\limits_{i=1}^{N} x_i(t), \lim\limits_{N\to\infty} \frac{1}{N}\sum\limits_{i=1}^{N} y_i(t), \lim\limits_{N\to\infty} \frac{1}{N}\sum\limits_{i=1}^{N} z_i(t))$, system (1) becomes:

$$\begin{aligned}
\dot{x}_i(t) &= y_i(t) \\
\dot{y}(t) &= -x_i(t) + \Phi(m_y+\nu) - \Phi(\nu) + \frac{1}{1!}\left[\Phi'(m_y+\nu)\right][y_i(t)-m_y] + \frac{1}{2!}\left[\Phi''(m_y+\nu)\right][y_i(t)-m_y]^2 \\
&\quad + \frac{1}{3!}\left[\Phi'''(m_y+\nu)\right][y_i(t)-m_y]^3 + \frac{1}{4!}\left[\Phi^{(4)}(m_y+\nu)\right][y_i(t)-m_y]^4 + K[m_x(t-\tau)-x_i(t)] + Z_i(t) \\
dZ_i(t) &= -\frac{Z_i(t)}{\varepsilon}dt + \sqrt{\frac{2D}{\varepsilon^2}}dW_i
\end{aligned} \tag{1A}$$

In order to derive mean-field approximate dynamical equations for starting system (1), we shall first suppose that: (a) dynamics is such that the distribution of x_i and y_i are Gaussian and (b) for large N the average over local random variables is given by the expectation with respect to the corresponding distribution, as in [9].

The cumulant analysis of a system (2) of above mentioned globally (all-to-all) coupled units shall be performed in the thermodynamic limit of an infinitely large ensemble, N→∞.

We introduce deviations from the mean-field: $\langle x(t)\rangle = \lim\limits_{N\to\infty} \frac{1}{N}\sum_{i=1}^{N} x_i(t)$, $\langle y(t)\rangle = \lim\limits_{N\to\infty} \frac{1}{N}\sum_{i=1}^{N} y_i(t)$, $\langle z(t)\rangle = \lim\limits_{N\to\infty} \frac{1}{N}\sum_{i=1}^{N} z_i(t)$, for each element $n_x(t) = \langle x(t)\rangle - x_i(t), n_y(t) = \langle y(t)\rangle - y_i(t), n_z(t) = \langle z(t)\rangle - z_i(t)$.

We assume that these fluctuations are Gaussian and statistically independent in different elements.

There is a set of moments known as cumulants [10,11] or Thiele semi-invariants which have an important property that all of them, for the third order, vanish in the Gaussian case.

Next, we introduce the following notation for the first and the second order cummulants:

- The means: $m_x(t) = \langle x(t)\rangle,\ m_x(t-\tau) = \langle x(t-\tau)\rangle, m_y(t) = \langle y(t)\rangle, m_z(t) = \langle z(t)\rangle$,
- The mean square deviations: $s_x(t) = \langle n_x^2(t)\rangle,\ s_y(t) = \langle n_y^2(t)\rangle, s_z(t) = \langle n_z^2(t)\rangle$,
- The cross-cummulants: $U_{xy}(t) = \langle n_x n\rangle_y,\ U_{xz}(t) = \langle n_x n_z\rangle, U_{yz}(t) = \langle n_y n_z\rangle$

By applying Ito's formula (or Ito's chain rule):

$dX = Fdt + GdW$

$Y(t) = U(x,t)$

$dY = \frac{\partial U}{\partial t}dt + \frac{\partial U}{\partial x}dX + \frac{1}{2}\frac{\partial^2 U}{\partial x^2}G^2 dt$

from Eq. (1A), following the procedure described in [9,12] one obtains:

$$\dot{m}_x = m_y \tag{2A}$$

$$\dot{m}_y = -m_x - a\ln(m_y+\nu) + a\ln(\nu) + \frac{1}{2}\frac{a}{(m_y+\nu)^2}s_y + \frac{3}{4}\frac{a}{(m_y+\nu)^4}{s_y}^2 + K(m_x(t-\tau)-m_x) + m_z \tag{3A}$$

$$\dot{m}_z = -\frac{1}{\varepsilon}m_z \tag{4A}$$

$$\begin{aligned} \dot{s}_x &= \langle n_x^2\rangle = \left\langle \overline{(\langle x\rangle - x_i)^2}^{\,\cdot} \right\rangle = \left\langle \overline{m_x^2 - 2m_x x_i + x_i^2}^{\,\cdot} \right\rangle = -\dot{m}_x^2 + \left\langle \dot{x}_i^2\right\rangle = -\dot{m}_x^2 + \left\langle \dot{x}_i^2\right\rangle = -2m_x\dot{m}_x + \langle 2x_i\dot{x}_i\rangle \\ &= -2m_x m_y + \langle 2x_i y_i\rangle = 2U_{xy} \Rightarrow \frac{1}{2}\dot{s}_x = U_{xy} \end{aligned} \tag{5A}$$

$$\begin{aligned} \dot{s}_y &= \langle \dot{n}_y^2\rangle = \left\langle \overline{(\langle y\rangle - y_i)^2}^{\,\cdot} \right\rangle = \left\langle \overline{m_y^2 - 2m_y y_i + y_i^2}^{\,\cdot} \right\rangle = -\dot{m}_y^2 + \langle \dot{y}_i^2\rangle = -2m_y\dot{m}_y + \langle 2y_i\dot{y}_i\rangle = \\ &= -2m_y\Big[-m_x + \Phi(m_y+\nu) - \Phi(\nu) + \frac{1}{2}\big[\Phi''(m_y+\nu)\big]s_y + \frac{1}{24}\big[\Phi^{(4)}(m_y+\nu)\big]\cdot 3s_y^2 \\ &\quad + K[m_x(t-\tau) - m_x] + m_z\big] + 2\langle -x_i y_i + y_i\Phi(m_y+\nu) - y_i\Phi(\nu) + \big[\Phi'(m_y+\nu)\big]\cdot \\ &\quad \cdot\big[y_i^2 - m_y y_i\big] + \frac{1}{2}\big[\Phi''(m_y+\nu)\big]\cdot\big[y_i\big(y_i^2 - 2y_i m_y + m_y^2\big)\big] + \frac{1}{6}\big[\Phi'''(m_y+\nu)\big]\cdot \\ &\quad \cdot\big[y_i\big(y_i^3 - 3y_i^2 m_y + 3y_i m_y^2 - m_y^3\big)\big] + \frac{1}{24}\big[\Phi^{(4)}(m_y+\nu)\big]\cdot \\ &\quad \cdot\big[y_i\big(y_i^4 - 4y_i^3 m_y + 6y_i^2 m_y^2 - 4y_i m_y^3 + m_y^4\big)\big] + K[y_i - m_x(t-\tau) - y_i x_i] + y_i z_i\rangle \\ &= -2U_{xy} + 2\big[\Phi'(m_y+\nu)\big]s_y + \frac{1}{3}\big[\Phi'''(m_y+\nu)\big]3s_y^2 - 2KU_{xy} + 2U_{yz} \\ &\quad \Rightarrow \frac{1}{2}\dot{s}_y = s_y\Big[\Phi'(m_y+\nu) + \frac{1}{2}\Phi'''(m_y+\nu)s_y\Big] - (K+1)U_{xy} + U_{yz} \\ &\quad \dot{s}_z = -\dot{m}_z^2 + \langle \dot{z}_i^2\rangle + \frac{2D}{\varepsilon^2} = -2m_z\dot{m}_z + \langle 2z_i\dot{z}_i\rangle + \frac{2D}{\varepsilon^2} \\ &= -2m_z\cdot\left(-\frac{1}{\varepsilon}m_z\right) + \left\langle 2z_i\left(-\frac{z_i}{\varepsilon} + \sqrt{\frac{2D}{\varepsilon^2}}dWi\right)\right\rangle + \frac{2D}{\varepsilon^2} \\ &= -\frac{2}{\varepsilon}s_z + \frac{2D}{\varepsilon^2} \\ &\quad \Rightarrow \frac{1}{2}\dot{s}_z = -\frac{1}{\varepsilon}s_z + \frac{D}{\varepsilon^2} \end{aligned} \tag{6A}$$

Last equation can be solved in order to obtain $s_z = (s_{z_0} - \frac{D}{\varepsilon})e^{-\frac{2}{\varepsilon}t} + \frac{D}{\varepsilon}$, where s_{z0} is an integration constant. It is obvious when $t\to\infty$, $s_z\to D/\varepsilon$, and because of that we fix the value for s_z to be exactly D/ε.

$$\begin{aligned} \dot{U}_{xy} &= \left\langle \overline{n_x n_y}^{\,\cdot}\right\rangle = \langle (m_x - x_i)\cdot(m_y - y_i)\rangle = \left\langle \overline{m_x m_y - m_x y_i - x_i m_y + x_i y_i}^{\,\cdot}\right\rangle = -\overline{m_x m_y}^{\,\cdot} + \left\langle \overline{x_i y_i}^{\,\cdot}\right\rangle \\ &= -m_x\dot{m}_y - m_y\dot{m}_x + \langle \dot{x}_i y_i\rangle + \langle x_i\dot{y}_i\rangle \\ &= -m_x\cdot\Big[-m_x + \Phi(m_y+\nu) - \Phi(\nu) + \frac{1}{2}\Phi''(m_y+\nu)\cdot s_y + \\ &\quad + \frac{1}{24}\Phi^{(4)}(m_y+\nu)\cdot 3s_y^2 + K\cdot[m_x(t-\tau) - m_x] + m_z\Big] - m_y m_y + \langle y_i^2\rangle \\ &\quad + \left\langle -x_i^2 + x_i\Phi(y_i+\nu) - x_i\Phi(\nu) + \frac{K}{N}\sum_{j=1}^{N}\left(x_j(t-\tau)x_i - x_i^2\right) + x_i z_i\right\rangle \\ &= m_x^2 - m_x\Phi(m_y+\nu) + m_x\Phi(\nu) - m_x\frac{1}{2}\Phi''(m_y+\nu)s_y - \\ &\quad - m_x\frac{1}{24}\Phi^{(4)}(m_y+\nu)\cdot 3s_y^2 - Km_x m_x(t-\tau) + Km_x^2 - m_x m_z - m_y^2 + s_y + m_y^2 - s_x \end{aligned}$$

$$
\begin{aligned}
&-m_x^2 + \Big\langle m_x \cdot \Phi(m_y+\nu) + +\Phi'(m_y+\nu)\cdot(x_i y_i - x_i m_y) + \frac{1}{2}\Phi''(m_y+\nu)\cdot\left(x_i y_i^2 - 2x_i y_i m_y + x_i m_y^2\right)\\
&+\frac{1}{6}\Phi'''(m_y+\nu)\left(x_i y_i^3 - 3x_i y_i^2 m_y + 3x_i y_i m_y^2 - x_i m_y^3\right) + \frac{1}{24}\Phi^{(4)}(m_y+\nu)\left(x_i y_i^4 - 4x_i y_i^3 m_y + 6x_i y_i^2 m_y^2 - 4x_i y_i m_y^3 + x_i m_y^4\right) - m_x\Phi(\nu)\\
&+K m_x m_x(t-\tau) - K s_x - K m_x^2 + U_{xz} + m_x m_z\Big\rangle\\
&= s_y - s_x + \Phi'(m_y+\nu)U_{xy} + \frac{1}{6}\Phi'''(m_y+\nu)3s_y U_{xy}\\
&-K s_x + U_{xz} \Rightarrow \dot{U}_{xy} = U_{xy}\left[\Phi'(my+\nu) + \frac{1}{2}\Phi'''(my+\nu)s_y\right] - (K+1)s_x + s_y + U_{xz}
\end{aligned}
\tag{7A}
$$

$$
\begin{aligned}
\dot{U}_{xz} &= \left\langle \dot{\overline{n_x n_z}}\right\rangle = \left\langle \dot{\overline{(m_x - x_i)(m_z - z_i)}}\right\rangle = \left\langle \dot{\overline{m_x m_z - m_x z_i - m_z x_i + x_i z_i}}\right\rangle =\\
&= \left\langle \dot{\overline{m_x m_z}}\right\rangle + \left\langle \dot{\overline{x_i z_i}}\right\rangle = -\dot{m}_x m_z - m_x \dot{m}_z + \langle \dot{x}_i z_i\rangle + \langle x_i \dot{z}_i\rangle = -m_y m_z -\\
&-m_x\left(-\frac{1}{\varepsilon}m_z\right) + \langle y_i z_i\rangle + \left\langle x_i\left(-\frac{z_i}{\varepsilon}\right) + x_i\sqrt{\frac{2D}{\varepsilon^2}}dW_i\right\rangle\\
&\Rightarrow \dot{U}_{xz} = U_{yz} - \frac{1}{\varepsilon}U_{xz}
\end{aligned}
\tag{8A}
$$

$$
\begin{aligned}
\dot{U}_{yz} &= \left\langle \dot{\overline{n_y n_z}}\right\rangle = \left\langle \dot{\overline{(m_y - y_i)(m_z - z_i)}}\right\rangle = \left\langle \dot{\overline{m_y m_z - m_y z_i - m_z y_i + y_i z_i}}\right\rangle =\\
&= \left\langle \dot{\overline{m_y m_z}}\right\rangle + \left\langle \dot{\overline{y_i z_i}}\right\rangle = -\dot{m}_y m_z - m_y \dot{m}_z + \langle \dot{y}_i z_i\rangle + \langle y_i \dot{z}_i\rangle =\\
&-m_z\Big[-m_x + \Phi(m_y+\nu) - \Phi(\nu) + \frac{1}{2}\Phi''(m_y+\nu)\cdot s_y + \frac{1}{24}\Phi^{(4)}(m_y+\nu)3s_y^2\\
&+K m_x(t-\tau) - K m_x + m_z\Big] - m_y\left(-\frac{1}{\varepsilon}m_z\right) + \Big\langle -x_i z_i + z_i\Phi(m_y+\nu) - z_i\Phi(\nu)\\
&+\Phi'(m_y+\nu)(y_i z_i - m_y z_i) + \frac{1}{2}\Phi''(m_y+\nu)\left(z_i y_i^2 - 2z_i y_i m_y + z_i m_y^2\right)\\
&+\frac{1}{6}\Phi'''(m_y+\nu)\left(z_i y_i^3 - 3z_i y_i^2 m_y + 3z_i y_i m_y^2 - z_i m_y^3\right) +\\
&+\frac{1}{24}\Phi^{(4)}(m_y+\nu)\cdot\left(z_i y_i^4 - 4z_i y_i^3 m_y + 6z_i y_i^2 m_y^2 - 4z_i y_i m_y^3 + z_i m_y^4\right) + K z_i m_x(t-\tau) -\\
&-K z_i x_i + z_i^2\Big\rangle + \left\langle y_i\left(-\frac{1}{\varepsilon}z_i\right) + y_i\sqrt{\frac{2D}{\varepsilon^2}}dW_i\right\rangle = -U_{xz} + \Phi'(m_y+\nu)U_{yz} + \frac{1}{6}\Phi'''(m_y+\nu)\cdot 3s_y U_{yz}\\
&-KU_{xz} + s_z - \frac{1}{\varepsilon}U_{yz}
\end{aligned}
\tag{9A}
$$

Eqs. (2A)–(9A) together compose the mean-field system of equations for earthquake nucleation model with colored noise:

$$
\begin{aligned}
&\dot{m}_x = m_y\\
&\dot{m}_y = -m_x - a\ln(m_y+\nu) + a\ln(\nu) + \frac{1}{2}\frac{a}{(m_y+\nu)^2}s_y + \frac{3}{4}\frac{a}{(m_y+\nu)^4}{s_y}^2 + K(m_x(t-\tau) - m_x) + m_z\\
&\dot{m}_z = -\frac{1}{\varepsilon}m_z\\
&\frac{1}{2}\dot{s}_x = U_{xy}\\
&\frac{1}{2}\dot{s}_y = s_y\left[-\frac{a}{m_y+\nu} - \frac{a}{(m_y+\nu)^3}s_y\right] - (K+1)U_{xy} + U_{yz}\\
&\dot{U}_{xy} = U_{xy}\left[-\frac{a}{m_y+\nu} - \frac{a}{(m_y+\nu)^3}s_y\right] - (K+1)s_x + s_y + U_{xz}\\
&\dot{U}_{xz} = U_{yz} - \frac{1}{\varepsilon}U_{xz}\\
&\dot{U}_{yz} = -U_{xz} - \frac{a}{m_y+\nu}U_{yz} - \frac{a}{(m_y+\nu)^3}s_y U_{yz} - KU_{xz} + D - \frac{1}{\varepsilon}U_{yz}
\end{aligned}
\tag{10A}
$$

which is the Eq. (3) in the main text.

References

[1] Corela C, Silveira G, Matias L, Schimmel M, Geissler WH. Ambient seismic noise tomography of SW Iberia integrating seafloor-and land-based data. Tectonophys 2017;700-701:131–49.
[2] Nakamura Y. A method for dynamic characteristics estimation of subsurface using microtremor on the ground surface. Quarterly Report of RTRI 1989:25–33.
[3] Briestensky M, Stemberk J, Michalık J, Bella P, Rowberry M. The use of a karstic cave system in a study of active tectonics: fault movements recorded at Driny Cave, Male Karpaty Mts (Slovakia). J Cave Karst Stud 2011;73:114–23.
[4] Ryberg T, Haberland Ch, Fuis GS, Ellsworth WL, Shelly DR. Locating non-volcanic tremor along the San Andreas Fault using a multiple array source imaging technique. Geophys J Int 2010;183:1485–500.
[5] Vasović N, Kostić S, Franović I, Todorović K. Earthquake nucleation in a stochastic fault model of globally coupled units with interaction delays. Comm Non Sci Numer Sim 2016;38:117–29.
[6] http://seismo.berkeley.edu/station_book/bks.html; 2018. [Accessed July 2018].
[7] Savin NE, White KJ. The Durbin-Watson test for serial correlation with extreme sample sizes or many regressors. Econometrica 1977;45:1989–96.
[8] De Sousa Vieira M. Chaos and synchronized chaos in an earthquake model. Phys Rev Lett 1999;82:201–4.
[9] Burić N, Ranković D, Todorović K, Vasović N. Mean field approximation for noisy delay coupled excitable neurons. Physica A 2010;389:3956–64.
[10] Lax M, Cai W, Xu M. Random processes in physics and finance. New York: Oxford University Press; 2006.
[11] Gardiner C. Stochastic methods: a handbook for the natural and social sciences. Berlin: Springer; 2009.
[12] Franović I, Todorović KD, Vasović N, Burić N. Stability, bifurcations, and dynamics of global variables of a system of bursting neurons. Chaos 2011;21:033109–1-9.